J. Astrophys. Astr. (2023) 44:47
https://doi.org/10.1007/s12036-023-09941-z

PAH emission features in star-forming regions and late type stars

RAHUL KUMAR ANAND[1], SHANTANU RASTOGI[1,*] and BRIJESH KUMAR[2]

[1]Department of Physics, DDU Gorakhpur University, Gorakhpur 273009, India.
[2]Aryabhatta Research Institute of Observational Sciences, Manora Peak, Nainital 263001, India.
*Corresponding author. E-mail: shantanu_r@hotmail.com

MS received 12 November 2022; accepted 9 January 2023

Abstract. Mid-infrared emission spectra, obtained from ISO archive, of thirteen astrophysical objects as well as computed spectra of 27 polycyclic aromatic hydrocarbon (PAH) molecules are studied. All the objects show strong aromatic infrared band (AIB) features with variations that correlate with object type. Based on AIB peak positions, the features for IRC +10216, Monoceros R2, and IC 5117 and PN-SwSt 1 are classified as type 'A', 'B' or 'C' for the first time. The AIBs at 6.2, 7.7 and 11.2 μm are used to obtain band intensity ratios for 6.2/7.7 and 11.2/6.2, which respectively indicate PAH size as number of carbon atoms and the ionization conditions of the medium. The smaller value of 6.2/7.7 points towards the presence of large PAH molecules, while higher value of 11.2/6.2 ratio relates to harsh conditions around the object. In general, for star-forming regions, the 6.2/7.7 band ratio obtained is >1 and the 11.2/6.2 ratio is >2, while for late type carbon stars, these values are <1 and <2. This indicates that small/medium-sized ionized PAHs are likely in star-forming regions and large PAHs in evolved stars. For each of the 27 plain PAH molecules, the integrated intensity in these bands is obtained from the computed infrared spectra and the band ratios are calculated. The ratio 6.2/7.7 in several computed medium and large sized PAH cations is in the range of observed ratio in most objects, but some molecules show large variations in band ratios, indicating that PAHs possible in interstellar medium could be more complex and with irregular structures.

Keywords. PAH—nebulae—mid-IR spectra—ISO.

1. Introduction

The presence of polycyclic aromatic hydrocarbon (PAH) molecules as indicated by the observation of aromatic infrared bands (AIBs) at 3.3, 6.2, 7.7, 8.6, 11.2 and 12.7 μm in a wide variety of astrophysical objects, points towards an interesting carbonaceous chemistry in space. Among the range of objects in which AIB features are observed, the more prominent ones are H II regions with young stars and active star formation; reflection nebulae, illuminated by bright background sources and planetary nebulae, which are late evolutionary stage of intermediate mass stars. The common feature in these objects is strong UV background. Yet, the AIB feature variations mark subtle differences (Peeters *et al.* 2002; Stock *et al.* 2016; Stock & Peeters 2017), which may be applied to probe the environment of the astrophysical object.

It is understood that the PAHs form in the outflows of AGB stars (Tielens 2008; Rastogi *et al.* 2013) by gas-phase chemical routes or on the surface of grains (Cherchneff *et al.* 1992; Van de Sande *et al.* 2019) and therefore, late type objects should show features belonging to fresh and large PAHs. These stable PAHs gradually move into the interstellar medium (ISM) and pass through several phases of dense-diffuse media, undergoing harsh radiation processing (Micelotta *et al.* 2010a, b; Tielens 2013). This leaves only the very stable medium-sized PAHs in molecular clouds and star-forming regions. In the strong radiations from star formation, there is also the possibility of PAHs released in the medium by grain fragmentation and etching (Pino *et al.* 2019). The scenario clearly indicates the possibility of different PAH populations in different objects.

Since the source of AIBs is a mixture of a family of PAHs present in an environment, the knowledge

This article is part of the Special Issue on "Star formation studies in the context of NIR instruments on 3.6m DOT".

Published online: 15 May 2023

Table 1. Basic details of selected objects.

Object	RA	DEC	Object type	Comments
Orion bar D2	05 35 21.40	−05 25 40.1	Star-forming region	Nebulae, HII region
Orion bar D5	05 35 19.81	−05 25 10.0	Star-forming region	Nebulae, HII region
Orion bar D8	05 35 18.22	−05 24 39.9	Star-forming region	Nebulae, HII region
Orion bar H2S1	05 35 20.31	−05 25 20.0	Star-forming region	Nebulae, HII region
NGC 2023	05 41 37.9	−02 15 52	Reflection nebulae	Illuminated by a massive young star named HD 37903
Mon R2	06 07 46.6	−06 22 59	Reflection nebulae	Chain of reflection nebulae illuminated by A- and B-type stars
IRC +10216	09 47 57.40	+13 16 43.56	AGB	Brightest; C-rich
CRL 915	06 19 58.21	−10 38 14.70	Post-AGB or pPNe	Prototype C-rich features
IC 5117	21 32 30.97	+44 35 47.5	PNe	C-rich, WR, one of the youngest PN
IRAS 21282+5050	21 29 58.47	+51 04 00.30	PNe	Compact PN, C-rich, WC11
PN-SwSt 1	18 16 12.27	−30 52 08.01	PNe	C/O < 1; WC 10
Hen 2-113	15 41 58.83	−56 36 25.6	PNe	Central star WC 10
IRAS 17047−5650	17 09 00.86	−56 54 48.09	PNe	C-rich, WC10

of the spectra of different families of PAHs (Langhoff 1996; Pathak & Rastogi 2005, 2006, 2007) is essential. Models of PAH mixtures that fit with observed profiles potentially lead to a better understanding of the chemical and physical evolutions of the astrophysical object (Pathak & Rastogi 2008). It is also important to understand the AIB variations and their relation with object types. With this objective, a variety of astrophysical objects having significant AIB signatures are studied. The infrared space observatory (ISO) archival data is used to obtain the mid-infrared (IR) emission features. The flux in different bands is obtained and ratios are analysed to understand object specific similarities and differences that may arise due to different PAH populations.

The computed spectral data of various PAH molecules have also been studied to find any correlation with mid-IR emission from different objects.

2. Astrophysical objects and their ISO spectra

Thirteen carbon-rich astrophysical objects are considered for the study. The basic information about these astrophysical objects is shown in Table 1. Based on their evolutionary status, similar stage objects are grouped together. The first group consist of four regions of star formation in the Orion nebula, the second group contains two reflection nebulae, which are illuminated by A- and B-type stars. Two carbon-rich objects, an AGB and a post-AGB star, which are popular and known for their molecular richness, are selected in the third group. The last group contains five well-studied planetary nebulae with Wolf–Rayet (WR) type central star. These constitute wide variety of objects and hence, form a suitable collection for the study towards understanding the AIB variations with object type.

Orion nebula is one of the brightest active star-forming region in sky which is located at ∼1500 light year and can be seen by naked eyes. This nebula is also known as Orion complex, consisting of several molecular clouds (Maddalena *et al.* 1986). Four different regions of this Orion complex have been chosen for their mid-IR emission studies. The object IRC +10216 is a carbon-rich AGB star embedded in a thick dusty envelope. Large number of molecules, detected in the ISM, are present in this object. The atmosphere in the last group of planetary nebulae, which have WR central star, have varying C/O ratios. Some such objects indicate a double dust chemistry, i.e., the circumstellar medium shows silicate features, indicative of oxygen-rich environment, as well as features corresponding to organic molecules pointing to a carbon-rich envelope (Szczerba *et al.* 2001; Marco & Soker 2002).

The mid-IR normalized spectral data for all the selected objects (Table 1) have been taken from Short Wavelength Spectrometer (SWS) archive (de Graauw *et al.* 1996), which are the part of ISO archive data center at European Space Agency. The instrument SWS of ISO covers the spectral range between 2.4 and 45.4 μm. The relevant PAH mid-IR spectral range between 2.5 and 15 μm is selected for the study of these objects. The normalized SWS spectra are well processed, but

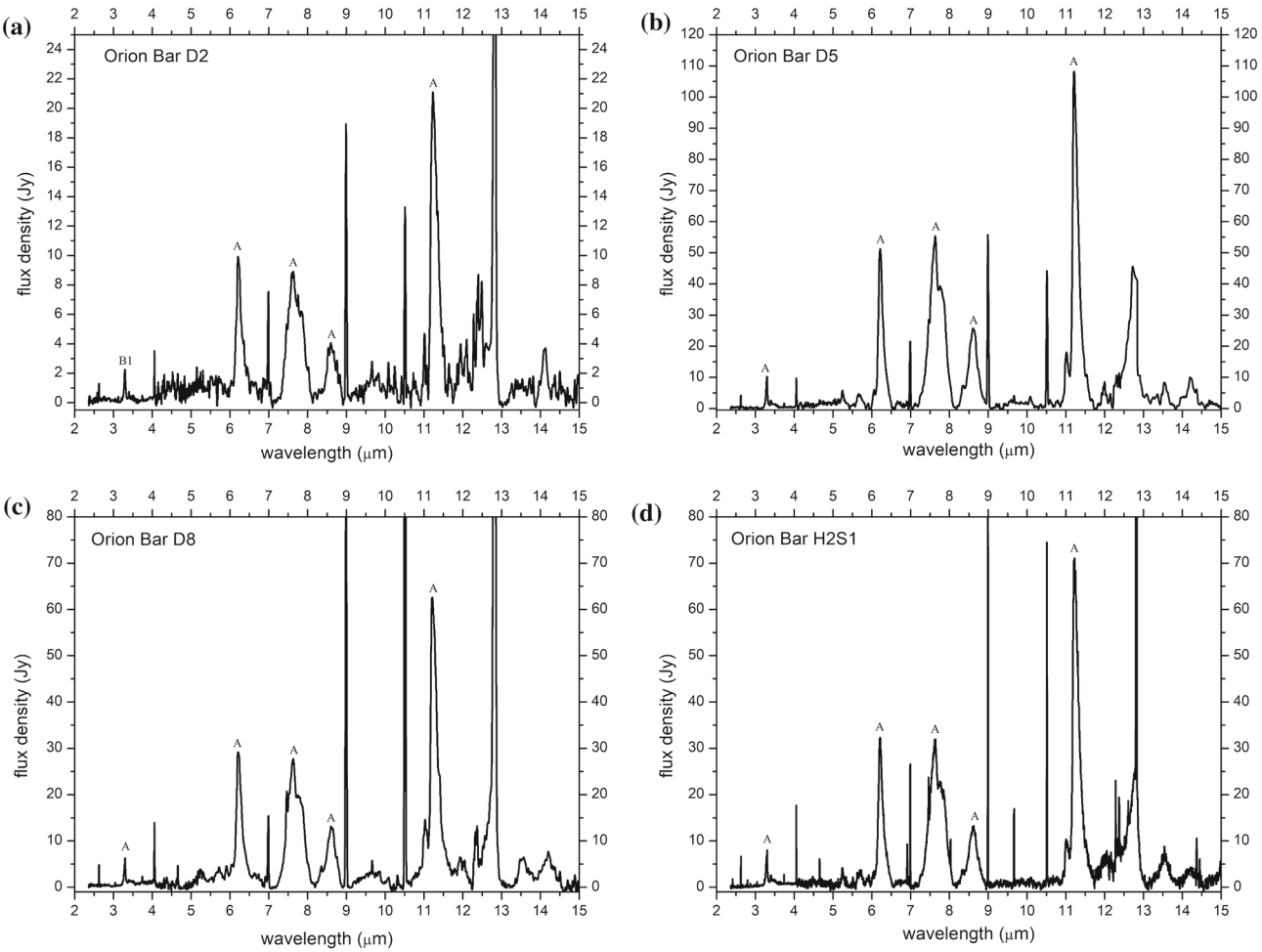

Figure 1. Mid-IR emission features of four Orion bar regions.

not continuum subtracted (Sloan *et al.* 2003), hence, it is important to remove the background from each spectrum before analysis. In most of the ISO range, the extinction is negligible (Pottasch & Beintema 1999), hence, no corrections for it, are considered. Local continuum spline fitting is used for all the spectra. A base line is obtained by using adjacent average method and relative intensity of emission features are computed. The continuum subtracted spectra of all the selected objects are shown in Figures 1–4.

The AIB features are evident in the spectra of nearly all the objects. There is variation both in peak position and relative intensity of the mid-IR bands. The variations are particularly evident in the prominent 7.7 μm band complex. Table 2 lists all the AIB positions and corresponding flux in each object. In all the objects, there is smaller flux in the 3.3 μm C–H stretching vibration mode compared to that in the modes between 6.0 and 12.0 μm. The solo C–H out-of-plane vibrational mode at 11.2 μm, is the strongest feature in most of the objects.

The band shape and peak positions of the AIBs correlate very well with object type. Based on the study of a large variety and number of objects, a classification scheme is developed for peaks lying between 6 and 9 μm regions by Peeters *et al.* (2002) and for the complete 3–12 μm range by van Diedenhoven *et al.* (2004). In general, features are placed in class A, when the band peaks are on the higher frequency end. As the band peak shifts to lower frequencies, it is placed in class B and then in class C. For each selected object, the class corresponding to every AIB is given in Table 2. For objects IRC +10216, Monoceros R2, IC 5117 and PN-SwSt 1, no classification is reported. Class categorization of these objects is made (in bold face) based on similarity of band shape and peak position wherever possible.

The C–H stretch vibration is prominently identifiable in all the Orion objects. The band shape and position of the 3.3 μm AIB in Orion bar H2S1 is a prototype for class A (van Diedenhoven *et al.* 2004) and most objects show similar profile. The Orion bar D2 region appears to

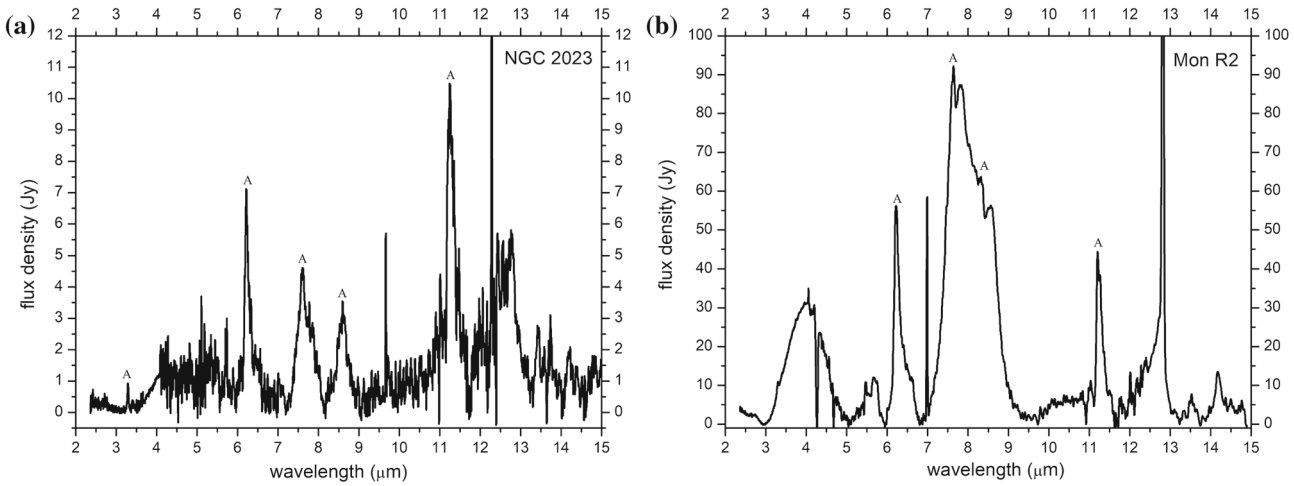

Figure 2. Mid-IR emission features of two reflection nebulae.

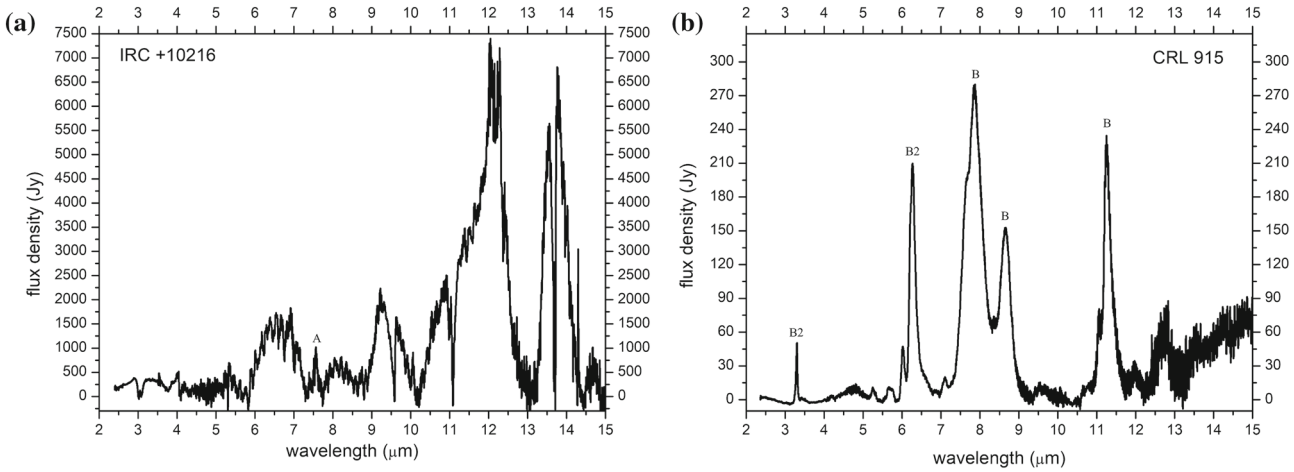

Figure 3. Mid-IR emission features AGB and post AGB stars.

have a similar class A profile. But high resolution observation (de Graauw *et al.* 1996) shows that in Orion bar D2, the blue wing of the band and the peak position are slightly shifted to the red. Hence, it is classified under B1 (van Diedenhoven *et al.* 2004). The reflection nebula Mon R2 is considered to be a template of high-UV and high-density photodissociation regions (PDRs), similar to the Orion bar (Berné *et al.* 2009). In this source, the 3.3 μm feature appears as a shoulder in a broad emission band, which could be due to high density and/or contribution of aliphatic C–H stretching. In IRC +10216, the AIB is not obvious and there appears an aliphatic peak near 3.5 μm. The metal poor post-AGB CRL 915 (HD 44179) has class B2 profile. The young planetary nebula IC 5117 shows a profile similar to CRL 915 and hence, placed in class B2. Due to profile similarity PN-SwSt 1 is also classified under B2.

In the 6–9 μm range, there are three important features: The 6.2 μm AIB related to the ring C–C stretch vibration, the 7.7 μm complex due to aromatic C–C stretch and C–H in-plane bend modes and the 8.6 μm band related to C–H in-plane bend vibrations. In all the star-forming regions and regions illuminated by young A and B type stars (reflection nebulae), these band profiles are of class A. Only in late type post AGB objects, the profile is of class B and in very few cases, it is of class C (Peeters *et al.* 2002; Maurya & Rastogi 2015). The youngest planetary nebula IC 5117 shows profiles closer to class B (Wada *et al.* 2003). In PN-SwSt 1, the profiles of 6.2 and 7.7 μm bands are also placed in class B. There are several overlapping features and noise in both these objects preventing classification of all AIBs. The only exception is IRAS 21282+5050 that shows class A type features. It is a compact pre-planetary nebula that probably contains a cool binary companion (Hsia *et al.* 2019). It remains to be studied if the presence of binary causes accretion that could be responsible for a PAH population different from other planetary nebulae.

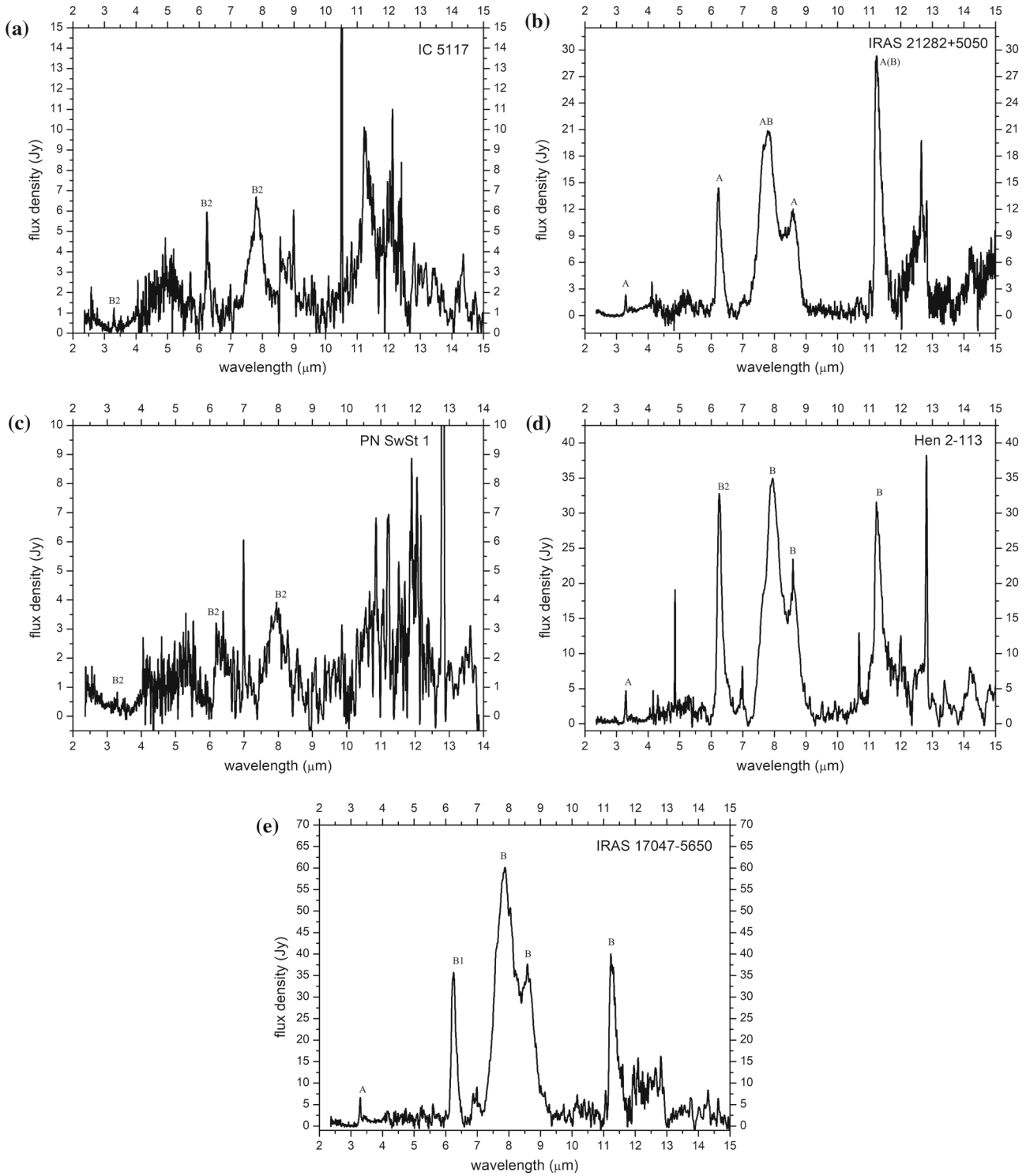

Figure 4. Mid-IR emission features of five planetary nebulae.

The 7.7 μm band appears to be a composite and decomposes into two sub-features at 7.8 and 7.6 μm (Peeters *et al.* 2002). The 7.7 μm feature is a result of C–H bending + C–C stretching, and is either dominant at 7.6 μm or peaks at 7.8–8 μm (Bregman 1989; Cohen *et al.* 1989). The theoretical spectra of large PAHs explain this feature, having two sub-components at 1285 and 1315 cm^{-1}, to be dependent on PAH size (Pathak & Rastogi 2007). Class A profile has a stronger 7.6 μm component and class B objects have stronger 7.8

Table 2. Mid-IR emission: Peak position and corresponding flux. Assigned AIB class is mentioned just below the peak value. The classification reported for the first time are in bold face.

Object	AIB 3.3 (μm)	Flux density (Jy)	AIB 6.2 (μm)	Flux density (Jy)	AIB 7.7 (μm)	Flux density (Jy)	AIB 8.6 (μm)	Flux density (Jy)	AIB 11.2 (μm)	Flux density (Jy)	AIB 12.7 (μm)	Flux density (Jy)
Orion bar D2	3.29 B1	2.252	6.21 A	9.918	7.63 A	8.911	8.60 A	4.064	11.23 A	21.102	*12.81*	*84.800*
Orion bar D5	3.29 A	10.1902	6.21 A	51.253	7.63 A	55.325	8.60 A	25.756	11.21 A	108.194	12.72	45.612
Orion bar D8	3.30 A	6.271	6.21 A	29.161	7.63 A	27.704	8.60 A	13.139	11.21 A	62.606	*12.81*	*332.496*
Orion bar H2S1	3.30 A	8.039	6.22 A	32.122	7.61 A	31.809	8.62 A	13.155	11.22 A	70.928	*12.81*	*476.028*
NGC 2023	3.28 A	0.918	6.21 A	7.117	7.60 A	4.615	8.59 A	3.549	11.26 A	10.441	12.76	5.809
Mon R2	3.30 –	10.917	6.22 **A**	56.199	7.64 **A**	92.186	8.56 **A**	56.324	11.20 **A**	44.330	*12.81*	*225.397*
IRC +10216	–	–	–	–	7.56 **A**	1018.408	–	–	11.28	2915.819	–	–
CRL 915	3.30 B2	50.503	6.27 B2	209.572	7.87 B	279.911	8.66 B	152.729	11.25 B	234.533	12.73	81.246
IC 5117	3.30 **B2**	1.233	6.24 **B2**	5.946	7.80 **B2**	6.697	8.56	4.736	11.22	10.118	12.80	4.428
IRAS 21282+5050	3.29 A	2.341	6.23 A	14.396	7.78 AB	20.866	8.55 A	11.768	11.24 A(B)	29.323	12.65	19.764
PN-SwSt 1	3.30 **B2**	0.831	6.26 **B2**	2.926	7.95 **B2**	3.919	8.63	1.749	11.23	6.935	*12.81*	*45.813*
Hen 2-113	3.29 A	4.689	6.25 B2	32.791	7.94 B	34.962	8.58 B	23.429	11.23 B	31.577	*12.81*	*38.191*
IRAS 17047−5650	3.29 A	6.645	6.25 B1	35.731	7.87 B	60.144	8.59 B	37.649	11.23 B	39.994	12.64	13.568

μm component. Thus, it is interpreted that the benign regions of PNe are conducive to PAH formation leading to large PAHs and PAHs with side groups, while harsh star-forming regions can have only compact stable medium-sized PAHs (Pathak & Rastogi 2008).

The AIB at 11.2 μm is due to the out-of-plane C–H wag mode of solo peripheral hydrogen (Allamandola *et al.* 1989). Solo hydrogen is possible in large compact PAHs. Wag motion of duo, trio and quarto hydrogen fall at sequentially lower frequencies. Unlike other PAH vibrational modes, the C–H out-of-plane feature shows very little variation between a neutral PAH and its cation (Rastogi *et al.* 2013). This makes it an interesting reference band to study the ionization level of any astrophysical region. In most objects, the 11.2 μm AIB is the strongest feature. The exceptions being Mon R2, CRL 915, Hen 2-113 and IRAS 17047-5650, where the 7.7 μm band is the strongest. In PAHs, this mode involves the same atoms as those in the 3.3 μm mode and hence, their intensities may correlate. In harsh conditions, there is possibility of PAH fragmentation and dehydrogenation, thus reducing the number of solo H atoms. This will result in smaller intensity in both the modes. Since ionization greatly affects the C–H stretch mode intensity, hence, the 11.2 μm solo C–H out-of-plane band is a better indicator of ionization and dehydrogenation states of PAHs in the medium.

The next AIB due to duo C–H out-of-plane mode appears at 12.7 μm (Tielens 2008), which is identifiable in most of the selected objects reported in Table 2, sometimes merging with the atomic Ne II line at 12.8 μm. In five objects, i.e., Orion bar D5, NGC 2023, CRL 915, IRAS 21282+5050 and IRAS 21282+5650, this 12.7 μm AIB is visible, independent of the NeII line. The feature is not evident in IRC +10216 due to other complex emissions present in it. Compared to the strong UV source regions, the feature, if present, is not as sharp in late type objects. This is consistent with the observation (Hony *et al.* 2001) that star-forming regions have sharper 12.7 μm feature. For modeling the emission spectra using PAH spectral data base (Bauschlicher *et al.* 2018), this criteria needs to be considered during selection of PAH species.

3. Band ratios

3.1 *Band ratios in spectra of various objects*

The mutual flux ratio of different AIBs can provide useful insights into the PAH families and their proportions possible in different objects. In this regard, the flux ratio 11.2/6.2 provides a measure of the ionization

Table 3. Flux ratios.

Object	Flux ratio at	
	6.2/7.7	11.2/6.2
Orion bar D2	1.113	2.1277
Orion bar D5	0.926	2.1110
Orion bar D8	1.053	2.1469
Orion bar H2S1	1.010	2.2081
NGC 2023	1.542	1.4669
Mon R2	0.610	0.7888
IRC +10216	–	–
CRL 915	0.749	1.1191
IC 5117	0.888	1.7015
IRAS 21282+5050	0.690	2.0368
PN-SwSt 1	0.747	2.3691
Hen 2-113	0.938	0.9630
IRAS 17047−5650	0.594	1.1193

balance of the emitting region (Hony *et al.* 2001). It also provides constraints on the possible size of PAHs in a region (Boersma *et al.* 2006; Tielens 2008). In mid-IR spectra, the emission modes at 6.2 and 7.7 μm are the brightest iconic features, therefore, many studies have been performed to determine the size distribution of PAH molecules using these features in various astrophysical regions. The ratio 6.2/7.7 was introduced by Draine & Li (2001) to determine the size of PAHs molecules, using theoretical calculations based on number of C atoms. Rigopoulou *et al.* (2021) found that the 6.2/7.7 ratio tracks the number of carbon atoms and showed that the higher ratio value have less number of C atoms.

The integrated fluxes in 6.2, 7.7 and 11.2 μm bands are used to obtain the 6.2/7.7 and 11.2/6.2 band ratios in all the selected objects. These are presented in Table 3. The observed flux ratio 6.2/7.7 for the selected objects lies between 0.594 and 1.542. The star-forming regions of Orion and reflection nebulae (except MonR2) have a value >1 for the 6.2/7.7 band, while stars in late evolutionary stage have this ratio as <1. This indicates that the PAH molecules with higher number of carbon atoms would be present in late phase stars.

For the 11.2/6.2 band ratio, the star-forming regions of Orion have similar values i.e., >2, while reflection nebulae and others late carbon stars (excluding IRAS21282+5050 and PN-SwSt 1) have the ratio as <2. It is observed that the 11.2/6.2 ratio correlates with the hardness of radiation (Zang *et al.* 2022). A higher ratio indicates harsh conditions within that medium. This is consistent with the fact that star-forming regions have stronger radiation field.

3.2 *Band ratios in computed spectra of PAH molecules*

The band ratios in observed spectra should correlate with infrared spectral intensity ratio in PAH molecules possible in the environment of an astrophysical object. To obtain indications towards PAHs possible in different objects, computed spectral data of 27 plain PAH molecules (Pathak & Rastogi 2005, 2006, 2007) are considered and band ratio for relevant modes are obtained. The molecules are categorized into three groups based of their molecular structure and size. Group-1 consists of small catacondensed (linear and non-linear) PAHs and Group-2 contains pericondensed medium-sized PAHs. Large PAHs having 38–96 carbon atoms are categorized as Group-3.

The spectrum of a typical neutral PAH usually shows a very strong 3.3 μm C–H stretching feature and negligible intensity in 6.0–10.0 μm modes, related to C–C stretch and C–H in-plane bend motions. On the other hand, ionized PAHs show negligible strength in 3.3 μm and highly enhanced peaks in 6.0–10.0 μm range. Therefore, smaller flux in 3.3 μm AIB compared to 6.0–10.0 μm region bands indicate towards the dominance of ionized PAHs in all objects.

In this regard, the relative intensities at each frequency between 1270–1325 cm^{-1} (for 7.7 μm AIB) and 1500–1650 cm^{-1} (for 6.2 μm AIB) are binned to get total relative intensity for the complete band profile. To relate the AIB features with the computed spectra and to track the molecular size, relative intensity ratios of 6.2/7.7 have been analyzed for neutral PAH molecules as well as for the cations. The computed relative intensity ratios for each molecule are listed in Table 4.

There are large variations in the intensity ratios. Since the astrophysical emissions result from a mixture of PAHs, we neglect extremely high ratio values for discussion and a threshold ratio of <5 is considered. The 6.2/7.7 intensity ratio in Group-1 molecules lies between 0.13–2.46 and 0.34–2.92 for neutrals and cations, respectively. This ratio for Group-2 molecules ranges from 0.60 to 4.86 for neutral, and for cation, it lies between 0.32 and 4.56. The large PAH molecules in Group-3 have the 6.2/7.7 intensity ratio between 1.65–4.13 and 0.36–2.59 for neutrals and cations, respectively. Among the selected molecules, coronene cation has the weakest intensity at 7.7 μm.

The theoretical band ratios for the 11.2/6.2 feature are very much smaller than 1 for cations, while in neutrals, where in most molecules, the 6.2 μm band is

Table 4. Intensity ratios of plane PAH molecules.

	Neutral					Cation				
	Relative intensity			Ratio	Ratio	Relative intensity			Ratio	Ratio
Molecule name	6.2 μm	7.7 μm	11.2 μm	6.2/7.7	11.2/6.2	6.2 μm	7.7 μm	11.2 μm	6.2/7.7	11.2/6.2
Group-1 (catacondensed PAHs)										
Naphthalene - $C_{10}H_8$	0.15	0.09	–	1.67	–	0.07	0.04	–	1.75	–
Anthracene - $C_{14}H_{10}$	0.16	0.17	0.76	0.94	4.75	0.35	1.04	0.09	0.34	0.26
Phenanthrene - $C_{14}H_{10}$	0.32	0.13	0.12	2.46	0.38	1.78	1.26	0.03	1.41	0.02
Tetracene - $C_{18}H_{12}$	0.16	0.23	0.84	0.70	5.25	0.35	0.12	0.07	2.92	0.20
Chrysene - $C_{18}H_{12}$	0.15	0.13	–	1.15	–	1.81	0.07	0.05	25.86	0.03
3,4-Benzophenanthrene - $C_{18}H_{12}$	0.17	0.11	–	1.55	–	0.65	1.09	0.09	0.60	0.14
Pentacene - $C_{22}H_{14}$	0.03	0.23	0.86	0.13	28.67	0.09	0.05	0.02	1.80	0.22
Hexacene - $C_{26}H_{16}$	0.09	0.28	0.89	0.32	9.89	0.98	0.15	–	6.53	–
Heptacene - $C_{30}H_{18}$	0.07	0.36	0.95	0.19	13.57	1.00	0.06	–	16.67	–
Group-2 (pericondensed PAHs)										
Pyrene - $C_{16}H_{10}$	0.18	0.06	–	3.00	–	1.06	0.59	–	1.80	–
Triphenylene - $C_{18}H_{12}$	0.12	0.01	–	12.00	–	1.49	0.95	0.12	1.57	0.08
Perylene - $C_{20}H_{12}$	0.41	0.08	–	5.13	–	1.01	1.06	–	0.95	–
Benzo[e]pyrene - $C_{20}H_{12}$	0.22	0.09	0.09	2.44	0.41	1.29	1.59	0.06	0.81	0.05
Anthanthrene - $C_{22}H_{12}$	0.31	0.07	0.94	4.43	3.03	1.14	0.25	0.34	4.56	0.30
Coronene - $C_{24}H_{12}$	0.09	0.15	1	0.60	11.11	1.00	0.02	0.38	50.00	0.38
Bisanthene - $C_{28}H_{14}$	0.59	0.14	0.73	4.21	1.24	0.36	1.12	0.15	0.32	0.42
$C_{28}H_{14}$	0.04	0.03	0.57	1.33	14.25	0.50	1.00	0.18	0.50	0.36
$C_{30}H_{14}$	0.34	0.07	0.9	4.86	2.65	1.76	0.88	0.63	2.00	0.36
Ovalene - $C_{32}H_{14}$	0.31	0.25	0.99	1.24	3.19	1.47	0.97	0.39	1.52	0.27
Group-3 (large PAHs)										
$C_{38}H_{16}$	0.33	0.08	0.62	4.13	1.88	3.05	2.11	1.00	1.45	0.33
$C_{48}H_{18}$	0.33	–	0.69	–	2.09	3.56	1.81	0.99	1.97	0.28
$C_{57}H_{19}$	0.43	0.26	1	1.65	2.33	2.48	1.57	0.3	1.58	0.12
$C_{62}H_{20}$	0.66	0.16	0.71	4.13	1.08	1.32	0.51	0.33	2.59	0.25
$C_{66}H_{20}$	0.39	0.13	1	3.00	2.56	1.64	1.18	0.13	1.39	0.08
$C_{80}H_{22}$	0.33	0.08	0.85	4.13	2.58	2.00	0.91	0.29	2.20	0.15
$C_{90}H_{24}$	0.68	0.30	1	2.27	1.47	0.43	1.20	0.14	0.36	0.33
$C_{96}H_{24}$	0.18	0.09	1	2.00	5.56	2.65	1.23	0.24	2.15	0.09

weak or absent, some of the ratios are far greater than 1 (Table 4, columns 6 and 11). Since, in the ISM, there is a complex mix of neutral and ionized PAH species with different fractions in different astrophysical objects, the model emission spectrum is needed for suitable comparison.

4. Discussion

The variation in band profile of PAH spectra give the clues about the size of molecules, charge distribution and compositions as well as radiation field around PAH molecules. The molecular size play very vital role in terms of infrared band emission, the bands profile at longer wavelengths are contributed by the larger molecules, while shorter wavelengths emission are the result of small PAH molecules (Allamandola *et al.* 1989).

The flux ratio 11.2/6.2 band in the star-forming Orion regions show large and similar ratio of >2. This indicates that there are PAHs with higher solo hydrogens, which are compact and ∼50 Carbon atom PAHs. The 11.2/6.2 ratio is significantly <1 only in Mon R2, which is a high density photodissociation region. Such environments may have high degree of dehydrogenation. This ratio clearly indicates the radiation field strength of the medium.

The ratio 6.2/7.7 helps to understand the size of PAHs in various astrophysical environments. All the star-forming regions excluding Orion bar D5 and reflection nebula NGC 2023 have value >1, which indicates the presence of small-medium size PAH molecules in

their medium. All selected AGB, post-AGB and PNe have the value of 6.2/7.7 ratio <1, which indicates towards existence of large PAH molecules in their surrounding medium.

The ratio 6.2/7.7 in several computed medium and large PAH cations (Table 4), is in the range of observed ratio in most objects. But, in computed, spectra there is large variation compared to observations. This indicates that not all simple PAHs are possible in ISM and there could be complex and irregular PAH structures (Maurya & Rastogi 2015; Bauschlicher *et al.* 2018) in astrophysical environments.

5. Conclusions

AIB features of 13 different regions are studied in relation with AIB class and object type. The regions that have stronger background radiation tend to show class A type features, while late type objects like planetary nebulae show class B profiles. Interrelationship of flux in different bands gives insight into the ionization state and size of the PAHs in different regions. In H II regions and reflection nebulae, similar PAH population is indicated. Such PAHs are compact medium-sized (∼50 C atoms) with a high ionization fraction. The PAH populations in benign regions of late type objects appear to be more complex with no clear trend. This can be due to the possibility of fresh PAHs being formed, and eventually some of these may not survive to reach the sites of star formation.

Acknowledgements

This work is conducted under MoU between ARIES, Nainital and DDU Gorakhpur University. RKA acknowledges financial support from University Grants Commission, New Delhi, under the Rajiv Gandhi National Fellowship scheme.

References

Allamandola L. J., Tielens A. G. G. M., Barker J. R. 1989, The Astrophysical Journal Supplement Series 71, 733, https://doi.org/10.1086/191396

Bauschlicher C. W., Ricca A., Boersma C., Allamandola L. J. 2018, The Astrophysical Journal Supplement Series 234, 32, https://doi.org/10.3847/1538-4365/aaa019

Berné O., Fuente A., Goicoechea J. R., *et al.* 2009, The Astrophysical Journal Letter 706, L160, https://doi.org/10.1088/0004-637X/706/1/L160, arXiv:0910.3935

Boersma C., Hony S., Tielens A. G. G. M. 2006, Astronomy & Astrophysics 447, 213, https://doi.org/10.1051/0004-6361:20053904

Bregman J. D. 1989, Observations of HII regions and planetary nebulae: The infrared emission bands. In: Interstellar Dust (Netherlands: Springer) p. 109, https://doi.org/10.1007/978-94-009-2462-8_9

Cherchneff I., Barker J. R., Tielens A. G. G. M. 1992, The Astrophysical Journal 401, 269, https://doi.org/10.1086/172059

Cohen M., Tielens A. G. G. M., Bregman J., *et al.* 1989, The Astrophysical Journal 341, 246, https://doi.org/10.1086/167489

de Graauw T., Haser L. N., Beintema D. A., *et al.* 1996, Astronomy & Astrophysics 315, L49

van Diedenhoven B., Peeters E., Kerckhoven C. V., *et al.* 2004, The Astrophysical Journal 611, 928, https://doi.org/10.1086/422404

Draine B. T., Li A. 2001, The Astrophysical Journal 551, 807, https://doi.org/10.1086/320227, arXiv:astro-ph/0011318

Hony S., Van Kerckhoven C., Peeters E., *et al.* 2001, Astronomy & Astrophysics 370, 1030, https://doi.org/10.1051/0004-6361:20010242, arXiv:astro-ph/0103035

Hsia C. H., Zhang Y., Kwok S., Chau W. 2019, Astrophysics and Space Science 364, 32, https://doi.org/10.1007/s10509-019-3523-2, arXiv:1902.08851

Langhoff S. R. 1996, The Journal of Physical Chemistry 100, 2819, https://doi.org/10.1021/jp952074g,

Maddalena R. J., Morris M., Moscowitz J., Thaddeus P. 1986, The Astrophysical Journal 303, 375, https://doi.org/10.1086/164083

Marco O. D., Soker N. 2002, Publications of the Astronomical Society of the Pacific 114, 602, https://doi.org/10.1086/341691

Maurya A., Rastogi S. 2015, Spectrochimica Acta Part A: Molecular and Biomolecular Spectroscopy 151, 1, https://doi.org/10.1016/j.saa.2015.06.069, http://www.sciencedirect.com/science/article/pii/S1386142515300093

Micelotta E. R., Jones A. P., Tielens A. G. G. M. 2010a, Astronomy & Astrophysics 510, A37, https://doi.org/10.1051/0004-6361/200911683, arXiv:0912.1595

Micelotta E. R., Jones A. P., Tielens A. G. G. M. 2010b, Astronomy & Astrophysics 510, A36, https://doi.org/10.1051/0004-6361/200911682, arXiv:0910.2461

Pathak A., Rastogi S. 2005, Theoretical IR spectra of large PAHs in study of UIR features. In: eds Lis D. C., Blake G. A., Herbst E. Astrochemistry: Recent Successes and Current Challenges, IAU Symposium, Vol. 231, p. 72

Pathak A., Rastogi S. 2006, Theoretical spectra of PAHs in modeling astrophysical IR features. In: 36th COSPAR Scientific Assembly, Vol. 36, p. 432

Pathak A., Rastogi S. 2007, Advances in Space Research 40, 1620, https://doi.org/10.1016/j.asr.2007.08.011

Pathak A., Rastogi S. 2008, Astronomy & Astrophysics 485, 735, https://doi.org/10.1051/0004-6361:20066618, arXiv:0804.2555

Peeters E., Hony S., Van Kerckhoven C., *et al.* 2002, Astronomy & Astrophysics, 390, 1089, https://doi.org/10.1051/0004-6361:20020773, arXiv:astro-ph/0205400

Pino T., Chabot M., Béroff K., *et al.* 2019, Astronomy & Astrophysics 623, A134, https://doi.org/10.1051/0004-6361/201834855

Pottasch S. R., Beintema D. A. 1999, Astronomy & Astrophysics 347, 975

Rastogi S., Pathak A., Maurya A. 2013, AIP Conference Proceedings 1543, 49, https://doi.org/10.1063/1.4812599,

Rigopoulou D., Barale M., Clary D. C., *et al.* 2021, Monthly Notices of the Royal Astronomical Society 504, 5287, https://doi.org/10.1093/mnras/stab959, https://academic.oup.com/mnras/article-pdf/504/4/5287/37975308/stab959.pdf

Sloan G. C., Kraemer K. E., Price S. D., Shipman R. F. 2003, The Astrophysical Journal Supplement Series 147, 379, https://doi.org/10.1086/375443

Stock D. J., Peeters E. 2017 Astrophysical Journal 837, 129, https://doi.org/10.3847/1538-4357/aa5f54

Stock D. J., Choi W. D. Y., Moya L. G. V, *et al.* 2016, Astrophysical Journal 819, 65, https://doi.org/10.3847/0004-637X/819/1/65

Szczerba R., Górny S. K., Stasińska G., Siódmiak N., Tylenda R. 2001, Astrophysics and Space Science 275, 113

Tielens A. 2008, Annual Review of Astronomy and Astrophysics 46, 289, https://doi.org/10.1146/annurev.astro.46.060407.145211

Tielens A. G. G. M. 2013, Reviews of Modern Physics 85, 1021, https://doi.org/10.1103/RevModPhys.85.1021

Van de Sande M., Sundqvist J. O., Millar T. J., Keller D., Decin L. 2019, The chemistry in clumpy AGB outflows. In: eds Kerschbaum F., Groenewegen M., Olofsson H., IAU Symposium, IAU Symposium, Vol. 343, p. 531, https://doi.org/10.1017/S1743921318005434

Wada S., Onaka T., Yamamura I., Murata Y., Tokunaga A. T. 2003, Astronomy & Astrophysics 407, 551, https://doi.org/10.1051/0004-6361:20030881, arXiv:astro-ph/0306309

Zang R. X., Maragkoudakis A., Peeters E. 2022, Monthly Notices of the Royal Astronomical Society, 511, 5142, https://doi.org/10.1093/mnras/stac214, https://academic.oup.com/mnras/article-pdf/511/4/5142/42699883/stac214.pdf